International Communications in Heat and Mass Transfer 109 (2019) 104373

Contents lists available at ScienceDirect

International Communications in Heat and Mass Transfer

journal homepage: www.elsevier.com/locate/ichmt

Heat and mass transfer in hollow-fiber modules for direct contact membrane distillation: Integral transforms solution and parametric analysis

Kleber Marques Lisboa[a,*], José Roberto Brito de Souza[a], Carolina Palma Naveira-Cotta[a], Renato Machado Cotta[a,b,c]

[a] Laboratory of Nano- and Microfluidics and Microsystems, LabMEMS Mechanical Engineering Dept. and Nanoengineering Dept., POLI & COPPE, Universidade Federal do Rio de Janeiro, Brazil
[b] Interdisciplinary Nucleus for Social Development, NIDES/CT, Technology Center, Universidade Federal do Rio de Janeiro, Brazil
[c] General Directorate of Nuclear and Technological Development, DGDNTM, Brazilian Navy, Rio de Janeiro, Brazil

ARTICLE INFO

Keywords:
Desalination
Direct contact membrane distillation
Waste heat recovery
Single domain formulation
Generalized integral transform technique

ABSTRACT

This work reports a heat and mass transfer analysis of direct contact membrane distillation (DCMD), aiming at predicting its performance in water desalination with hollow-fiber membrane modules. A single-fiber model is proposed to simulate the simultaneous heat and mass transfer in DCMD for a hollow-fibers bundle, and the efficiency of the desalination process is assessed. The problem for a single membrane is handled through the hybrid numerical-analytical approach known as the Generalized Integral Transform Technique (GITT). A comparison of the numerical results obtained with the proposed model and both theoretical and experimental results from the literature is carried out. A prediction of the performance of a hollow-fiber DCMD module is then presented and paths for further improvement are discussed.

1. Introduction

The increasing awareness of the impact of human activities on climate change and the rapid depletion of natural resources has pushed for the development of waste heat recovery technologies along the last three decades. To improve the overall energy efficiency of processes in industry, the recovery of high exergy waste heat is often done within the process itself. On the other hand, low exergy waste (*low-grade heat*) is difficult to recycle effectively due to the small temperature differences involved, which hinders the heat transfer needed for this purpose. However, alternatives for the reuse of low-grade heat are being sought after to further decrease the amount of energy wasted in industrial processes [1].

Motivated by the expansion of water stress within several communities around the world, effective ways to obtain potable water from brackish and seawater are being increasingly researched [2]. Amongst these alternatives, the Direct Contact Membrane Distillation (DCMD) is here highlighted. In this process, the distillation of water is driven by a vapor pressure difference across a hydrophobic micro- or nanoporous membrane in contact with hot brackish or seawater on one side and cold distilled water on the other [3–5]. The low pressures and temperatures involved in DCMD in comparison with reverse osmosis and other thermal desalination processes, respectively, renders this technology attractive for the use of low-grade waste heat recovery and solar energy in desalination processes [6,7].

Modeling and numerical solution of DCMD processes have been proven useful for the analysis of different design configurations and to characterize the porous membrane employed [8]. Most of the modeling effort is dedicated to determining the appropriate approach to estimate the mass transport of distillate across the membrane. For that purpose, the Dusty Gas Model (DGM) is usually employed, with only the Knudsen and molecular diffusion mechanisms being considered in DCMD applications [9]. The adequate model depends on the size of the pores of the membrane relative to the mean free path of the water vapor molecules, thus needing to be determined for each particular situation. Nonetheless, given the typical pore sizes of commercial membranes and operating conditions in DCMD, the transition model, considering that Knudsen and molecular diffusion occur simultaneously, has proven to be the most suitable one [10]. Furthermore, models for both of the most commonly employed module configurations, namely flat sheet [10] and hollow fiber [11] membrane modules, were developed.

Despite the ubiquitous presence of discrete numerical methods, e.g. finite differences and finite volumes methods, for the solution of partial differential models, analytical approaches are still useful for verification of numerical codes and arbitrarily precise calculations. However, analytical methods are usually restricted to linear problems in regular

* Corresponding author.
E-mail address: kleberlisboa@poli.ufrj.br (K.M. Lisboa).

https://doi.org/10.1016/j.icheatmasstransfer.2019.104373

Available online 15 November 2019

Nomenclature

a	activity coefficient
c_p	specific heat at constant pressure
d_p^*	mean pore diameter of the membrane
h_v	enthalpy of the water vapor
j_w	permeate water flux
k	thermal conductivity
k_{mem}	dimensionless thermal conductivity of the membrane
k_p^*	thermal conductivity of the polymer
M_w^*	molecular weight of water
N_{fbr}	number of fibers
P	partial pressure of water vapor
Pe	Péclet number
Q	volumetric flow rate
r	radial coordinate
r_e	external radius of the fiber
r_i	internal radius of the fiber
r_v^*	vessel radius
T	temperature
u	longitudinal velocity component
z	longitudinal coordinate

Greek letters

δ	Kronecker delta
ε	porosity of the membrane
λ,ω	eigenvalues corresponding to eigenfunctions ψ and Ω, respectively
ρ	density
τ	tortuosity
ψ	eigenfunction for temperature
Ω	auxiliary eigenfunction

Subscripts and superscripts

i,j	order of eigenquantities for the temperature
l	lumen side
m,n	order of auxiliary eigenquantities
s	shell side
w	water
$\sim$	normalized eigenfunction
$*$	dimensional quantity

geometries, hindering its widespread applicability. In this context, hybrid numerical-analytical methods were developed with the intent of incorporating analytical features into numerical methods. One of the most successful hybrid methods is the Generalized Integral Transform Technique (GITT), which has been applied to several convection-diffusion problems with nonlinear boundary conditions and source terms, irregular geometries, moving boundaries, etc. A more complete literature review of the GITT can be found in compilations published over the years [12,13]. Recently, a new strategy was proposed within the GITT framework to deal with problems in heterogeneous media and complex geometries. The so-called single domain reformulation consists of treating the different media as abruptly space-varying physical properties, avoiding numerous individual formulations for each region coupled by their common boundaries, thus markedly simplifying the modeling and solution processes. This approach was successfully applied to conjugated heat transfer [14], heat conduction in heterogeneous media [15], and to flow and mass transport in channels or cavities partially filled with porous media [16–18].

The present work is part of a project aimed at analyzing a hollow fiber membrane module for desalination of brackish water through numerical simulations and experiments with a desalination unit installed at the Federal University of Rio de Janeiro (UFRJ) [19]. The numerical simulation has been performed using the single domain formulation strategy [14–18] and the GITT approach to solve a single-fiber model of the heat and mass transfer phenomena involved. The results obtained with this hybrid computational-analytical approach are compared with numerical and experimental results from the literature. Furthermore, a brief analysis of the desalinated water fluxes in the UFRJ desalination unit is offered.

2. Modeling and solution methodology

2.1. Geometry and fluid flow

Hollow-fiber membrane modules usually consist of a bundle of membranes positioned in parallel with both the feed and permeate flows [11]. Directly modeling and simulating such bundles is often cumbersome from a computational standpoint. Therefore, in this work, a simpler single-fiber model, which is based on the one developed by Kim [11], is proposed. Fig. 1 depicts the geometry used in this single-fiber model, centered at the hollow-fiber membrane, with cold permeate and hot feed flowing in the innermost (lumen) and outermost (shell) portions of the proposed geometry, respectively. To maximize the mean radial temperature difference along the fiber, and thus the driving force for distillate flow through the membrane, only the counter-current configuration is considered. A cylindrical coordinate system and main geometrical parameters are included to ease the understanding of the model. Both the feed and permeate flows are

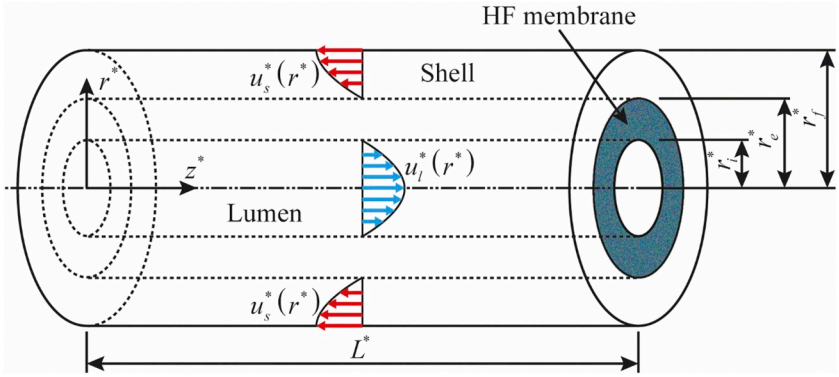

Fig. 1. Geometry for the single-fiber model of the hollow-fiber membrane module. A cylindrical coordinate system and the main dimensions are included. Fully developed flow profiles are indicated in both the shell and lumen sides.

considered to be fully developed and unaffected by the flow of distillate through the membrane, based on the assumption that the latter is much smaller than the former ones. At the external face of the cylinder, the tangential stress is considered to be null. The fully developed dimensionless velocity distributions in the lumen and shell sides are then given, respectively, by

$$u_l(r) = 2\hat{u}_l\left(1 - \frac{r^2}{r_i^2}\right) \tag{1.a}$$

$$u_s(r) = \frac{2(-1 + r_e^2)}{3 - 4r_e^2 + r_e^4 + 4\ln(r_e)}\hat{u}_s\left[-r^2 + r_e^2 + 2\ln\left(\frac{r}{r_e}\right)\right] \tag{1.b}$$

The dimensionless quantities are related to their dimensional counterparts as follows,

$$u_s = \frac{u_s^*}{u_m^*};\ u_l = \frac{u_l^*}{u_m^*};$$
$$\hat{u}_l = \frac{Q_l^*}{u_m^* N_{fbr}\pi r_i^{*2}};\ \hat{u}_s = \frac{Q_s^*}{u_m^* N_{fbr}\pi(r_f^{*2} - r_e^{*2})} \tag{2.a-d}$$

$$r = \frac{r^*}{r_f^*};\ r_i = \frac{r_i^*}{r_f^*};\ r_e = \frac{r_e^*}{r_f^*} \tag{2.e-g}$$

with the average velocity given by,

$$u_m^* = \frac{Q_l^* + Q_s^*}{N_{fbr}\pi[r_i^{*2} + (r_f^{*2} - r_e^{*2})]} \tag{2.h}$$

where u_l^* is the dimensional velocity profile in the lumen, u_s^* is the dimensional velocity profile in the shell, u_l is the dimensionless velocity profile in the lumen, u_s is the dimensionless velocity profile in the shell, u_m^* is the average velocity, Q_l^* is the flow rate in the lumen, Q_s^* is the flow rate in the shell, N_{fbr} is the number of fibers.

As for the size of the cylindrical region presented in Fig. 1, the transversal area of the cylinder is set to be equal to the transversal area of the vessel containing the bundle of membranes divided by the number of hollow fibers, in the form:

$$r_f^* = \frac{r_v^*}{\sqrt{N_{fbr}}} \tag{3}$$

where r_v^* is the radius of the vessel containing the hollow fibers.

2.2. Heat transfer model

A steady state convection-diffusion conjugated heat transfer model with single domain formulation is proposed to the single-fiber desalination module. The thermophysical properties of each material are considered to be constant. Assuming the Péclet numbers are sufficiently large, axial diffusion is neglected. A transversal advection term is included in the membrane region to represent the heat transported by the water vapor. The proposed model is presented below, in dimensionless form:

$$w\frac{\partial T}{\partial z} + \frac{\mathrm{Pe}}{r}\frac{\partial}{\partial r}[r\gamma j_w h_v] = \frac{1}{r}\frac{\partial}{\partial r}\left[rk\frac{\partial T}{\partial r}\right] \tag{4.a}$$

$$T(r, \phi(r)z_f) = \phi(r);\ T(0,z) = \text{finite};\ \left.\frac{\partial T}{\partial r}\right|_{r=1} = 0 \tag{4.b-d}$$

where,

$$w(r) = \begin{cases} u_l(r),\ 0 \le r < r_i \\ 0,\ r_i \le r \le r_e \\ -u_s(r),\ r_e < r \le 1 \end{cases};\ k(r) = \begin{cases} 1,\ 0 \le r < r_i \\ k_{mem},\ r_i \le r \le r_e \\ 1,\ r_e < r \le 1 \end{cases} \tag{4.e,f}$$

$$\gamma(r) = \begin{cases} 1,\ r_i \le r \le r_e \\ 0,\ r > r_e \text{ or } r < r_i \end{cases};\ \phi(r) = \begin{cases} 1,\ r_e \le r \le 1 \\ 0,\ r < r_e \end{cases} \tag{4.g,h}$$

The dimensionless quantities are obtained from their dimensional counterparts in the following way:

$$z = \frac{z^*}{\mathrm{Per}_f^*};\ T = \frac{T^* - T_l^*}{T_s^* - T_l^*};$$
$$w = \frac{\rho^* c_p^* u^*}{\rho_w^* c_{p,w}^* u_m^*};\ k = \frac{k^*}{k_w^*} \tag{5.a-d}$$

$$j_w = \frac{j_w^*}{\rho_w^* u_m^*};\ h_v = \frac{h_v^*}{c_{p,w}^*(T_s^* - T_l^*)};\ \mathrm{Pe} = \frac{\rho_w^* c_{p,w}^* u_m^* r_f^*}{k_w^*} \tag{5.e-g}$$

where T^* is the dimensional temperature, T is the dimensionless temperature, T_l^* is the entry temperature in the lumen side, T_s^* is the entry temperature in the shell side, M_w^* is the molecular weight of water, j_w^* is the dimensional distilled water flux, j_w is the dimensionless distilled water flux, h_v^* is the dimensional water vapor enthalpy, h_v is the dimensionless water vapor enthalpy, ρ_w^* is the density of water, c_p^* is the specific heat at constant pressure of water, and k_w^* is the thermal conductivity of water.

The thermal conductivity of the membrane is composed of the thermal conductivity of the polymer material and the thermal conductivity of the gas filling its voids. A few models are available to account for these two components in describing the effective thermal conductivity of the membrane. In this work, the model stemming from Maxwell's fundamental model is chosen [11], in the form,

$$k_{mem} = \frac{k_v^*}{k_w^*}\frac{1 + 2\beta(1 - \varepsilon)}{1 - \beta(1 - \varepsilon)} \tag{6.a}$$

with,

$$\beta = \frac{k_p^* - k_v^*}{k_p^* + 2k_v^*} \tag{6.b}$$

where k_v^* is the thermal conductivity of the water vapor, k_p^* is the thermal conductivity of the polymer, and ε is the porosity of the membrane.

The water vapor enthalpy can be determined, in dimensionless form, from the following correlation [20]:

$$h_v = h_0 + c_p T \tag{7.a}$$

$$h_0 = \frac{h_0^* + c_p^*[T_l^* + 273.15]}{M_w^* c_{p,w}^*(T_s^* - T_l^*)};\ c_p = \frac{c_p^*}{M_w^* c_{p,w}^*} \tag{7.b,c}$$

where M_w^* is the molecular weight of water, and,

$$h_0^* = 2024.3\ \frac{\mathrm{kJ}}{\mathrm{kg}};\ c_p^* = 1.7535\ \frac{\mathrm{kJ}}{\mathrm{kgK}} \tag{7.d,e}$$

2.3. Mass transfer model

A mass diffusion model is proposed for the water vapor transport through the membrane. Combined Knudsen-molecular diffusion is considered appropriate. Neglecting axial diffusion and with properties evaluated at the membrane average temperature, the following model, in dimensionless form, results:

$$\frac{1}{r}\frac{\partial}{\partial r}\left[r\frac{\partial P_v}{\partial r}\right] = 0 \tag{8.a}$$

$$P_v(r_i, z) = P_l(z);\ P_v(r_e, z) = P_s(z) \tag{8.b,c}$$

where,

$$P_l = (1 - x_{NaCl,l})a_l\frac{\exp\left(23.1964 - \frac{3816.44}{T_l^* + (T_s^* - T_l^*)T(r_i,z) + 227.02}\right)}{\rho_w^* u_m^{*2}} \tag{8.d}$$

$$P_s = (1 - x_{NaCl,s})a_s\frac{\exp\left(23.1964 - \frac{3816.44}{T_l^* + (T_s^* - T_l^*)T(r_e,z) - 227.02}\right)}{\rho_w^* u_m^{*2}} \tag{8.e}$$

where P_v is the dimensionless partial pressure of water vapor, P_l is the dimensionless partial pressure of water vapor at the lumen-membrane interface, P_s is the dimensionless partial pressure of water vapor at the shell-membrane interface, $x_{NaCl,\ l}$ is the mole fraction of NaCl at the lumen-membrane interface, $x_{NaCl,\ s}$ is the mole fraction of NaCl at the shell-membrane interface, a_l is the activity coefficient of water at the lumen-membrane interface, and a_s is the activity coefficient of water at the shell-membrane interface. The mole fractions of NaCl are assumed to be approximately constant throughout the channels, thus neglecting the concentration polarization effects. The activity coefficients are given by [11]:

$$a_l = 1 - 0.5x_{NaCl,l} - 10x_{NaCl,l}^2 \tag{9.a}$$

$$a_s = 1 - 0.5x_{NaCl,s} - 10x_{NaCl,s}^2 \tag{9.b}$$

Defining the dimensionless permeate water flux at the lumen-membrane interface as:

$$r_i j_w|_{r_i} = -r_i \frac{\varepsilon}{\tau} \frac{D_{eff}(T_{avg}) M_w^* u_m^{*2}}{R[T_l^* + (T_s^* - T_l^*)T_{avg}]} \frac{\partial P_v}{\partial r}\bigg|_{r=r_i} \tag{10.a}$$

with,

Molecular dimensionless diffusivity:

$$D_B(T) = \frac{1.8022 \times 10^{-10}}{u_m^* r_f^*} \{T_l^* + (T_s^* - T_l^*)T\}^{2.072} \tag{10.b}$$

Knudsen dimensionless diffusivity:

$$D_K(T) = \frac{d_p^*}{3u_m^* r_f^*} \sqrt{\frac{8R}{\pi M_w^*}} \sqrt{T_l^* + (T_s^* - T_l^*)T} \tag{10.c}$$

Effective dimensionless diffusivity:

$$D_{eff}(T) = \left(\frac{1}{D_B(T)} + \frac{1}{D_K(T)} \right)^{-1} \tag{10.d}$$

where τ is the membrane tortuosity, R is the universal gas constant, T_{avg} is the average temperature in the membrane, d_p^* is the mean membrane pore diameter.

Solving Eqs. (8.a–8.b,c) and substituting into Eq. (10.a), we then have:

$$r_i j_w|_{r_i} = \frac{\varepsilon}{\tau} \frac{D_{eff}(T_{avg}) u_m^{*2} M_w}{R[T_l^* + (T_s^* - T_l^*)T_{avg}] \ln(r_e/r_i)} (P_l - P_s) \tag{11}$$

Eq. (11) bears a sign convention for the permeate water flux. For the case under consideration, with the shell temperature and, consequently, the partial pressure of the shell side being larger than their counterparts in the lumen side, the local permeate flux is always negative.

2.4. Solution methodology

An eigenvalue problem, obtained from Eq. (4.a) without the vapor heat transport term through separation of variables, is chosen as basis for the eigenfunction expansion, in the form:

$$\frac{1}{r}\frac{d}{dr}\left[rk(r)\frac{d\psi_i}{dr} \right] + \lambda_i^2 w(r)\psi_i(r) = 0 \tag{12.a}$$

$$\psi_i(0) = \text{finite}; \quad \frac{d\psi_i}{dr}\bigg|_{r=1} = 0 \tag{12.b,c}$$

The GITT itself is proposed to handle the eigenvalue problem of Eqs. (12.a–12.b,c). For that purpose, a simpler eigenvalue problem is posed, in the form:

$$\frac{1}{r}\frac{d}{dr}\left[r\frac{d\Omega_m}{dr} \right] + \omega_m^2 \Omega_m(r) = 0 \tag{13.a}$$

with boundary conditions and normalization given by,

$$\Omega_m(0) = \text{finite}; \quad \frac{d\Omega_m}{dr}\bigg|_{r=1} = 0 \tag{13.b,c}$$

$$\widetilde{\Omega}_m(r) = \frac{\Omega_m(r)}{\sqrt{N_{\Omega,m}}}; \quad N_{\Omega,m} = \int_0^1 r\Omega_m(r)^2 dr \tag{13.d,e}$$

The solution to Eqs. (13.a–13.d,e) bears the following orthogonality property:

$$\int_0^1 r\widetilde{\Omega}_m(r)\widetilde{\Omega}_n(r)dr = \delta_{mn} \tag{14}$$

A transform-inverse pair is obtained with the aid of the orthogonality property of Eq. (14) as shown below:

$$\overline{\psi}_{i,m} = \int_0^1 r\widetilde{\Omega}_m(r)\psi_i(r)dr; \quad \psi_i(r) = \sum_{m=1}^{\infty} \overline{\psi}_{i,m}\widetilde{\Omega}_m(r) \tag{15.a,b}$$

Applying the operator $\int_0^1 r\widetilde{\Omega}_m(r)(\cdot)dr$ to Eq. (12.a), we then have,

$$\sum_{n=1}^{\infty} \{A_{mn} + \lambda_i^2 B_{mn}\}\overline{\psi}_{i,m} = 0 \tag{16.a}$$

with integral coefficients given by,

$$A_{mn} = -\omega_m^2 \delta_{mn} - \int_{r_i}^{r_e} r[k_{mem} - 1]\frac{d\widetilde{\Omega}_m}{dr}\frac{d\widetilde{\Omega}_n}{dr}dr \tag{16.b}$$

$$B_{mn} = \int_0^1 rw(r)\widetilde{\Omega}_m(r)\widetilde{\Omega}_n(r)dr \tag{16.c}$$

The algebraic eigenvalue problem is numerically solved, after

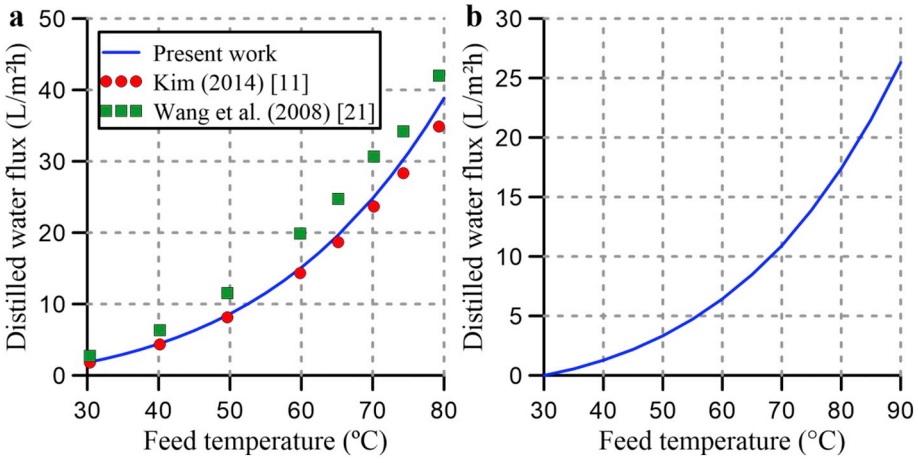

Fig. 2. Effect of the feed temperature on the distilled water flux. (a) numerical [11] and experimental [22] results from the literature; (b) distilled water flux prediction for the UFRJ desalination unit.

truncation to a finite order M, using IMSL's built-in function DGVCRG [21] in a Fortran code.

The eigenfunction ψ_i has the following orthogonality property:

$$\int_0^1 rw(r)\psi_i(r)\psi_j(r)dr = N_{\psi,i}\delta_{ij} \tag{17.a}$$

with a norm given by,

$$N_{\psi,i} = \int_0^1 rw(r)\psi_i(r)^2 dr \tag{17.b}$$

Proceeding with the GITT formalism, a transform-inverse pair is formed for the temperature field as shown below:

$$\overline{T}_i(z) = \frac{1}{N_{\psi,i}}\int_0^1 rw(r)\psi_i(r)T(r,z)dr;$$
$$T(r,z) = \sum_{i=1}^{\infty}\overline{T}_i(z)\psi_i(r) \tag{18.a,b}$$

Applying the operators $\frac{1}{N_{\psi,i}}\int_0^1 r\psi_i(r)(\cdot)dr$ to Eq. (4.a) and $\int_0^1 rw(r)\psi_i(r)(\cdot)dr$ to Eq. (4.b-d), we then have,

$$\frac{d\overline{T}_i}{dz} + \lambda_i^2\overline{T}_i(z) = \mathrm{Pe}(r_i j_w|_{r_i})\left\{h_0\overline{b}_i + c_p\sum_{j=1}^{\infty}E_{ij}\overline{T}_j(z)\right\} \tag{19.a}$$

$$\sum_{j=1}^{\infty}C_{ij}\overline{T}_j(0) + \sum_{j=1}^{\infty}D_{ij}\overline{T}_j(z_f) = \overline{f}_i \tag{19.b}$$

where,

$$C_{ij} = \int_0^{r_i} rw(r)\psi_i(r)\psi_j(r)dr \tag{19.c}$$

$$D_{ij} = \int_{r_e}^1 rw(r)\psi_i(r)\psi_j(r)dr \tag{19.d}$$

$$E_{ij} = \frac{1}{N_{\psi,i}}\int_{r_i}^{r_e}\frac{d\psi_i}{dr}\psi_j(r)dr \tag{19.e}$$

$$\overline{b}_i = \frac{1}{N_{\psi,i}}\int_{r_i}^{r_e}\frac{d\psi_i}{dr}dr;\quad \overline{f}_i = \int_{r_e}^1 rw(r)\psi_i(r)dr \tag{19.f,g}$$

Note that the product of the radius by the permeate flux is constant along the radial coordinate by virtue of the mass conservation principle, thus allowing it to be extracted from the integrals as in Eq. (19.a).

The system of ordinary differential equations of Eqs. (19.a–19.f,g) is then truncated to a finite order N and solved with a dedicated Fortran code using IMSL function DBVPFD [21]. The temperature field is then recovered with the aid of Eq. (18.b).

3. Results and discussion

Fig. 2a shows a comparison of the results of the developed model and solution methodology with previously published numerical [11] and experimental [22] results. The agreement with the numerical results of the distilled water flux provided by Kim [11] is quite reasonable

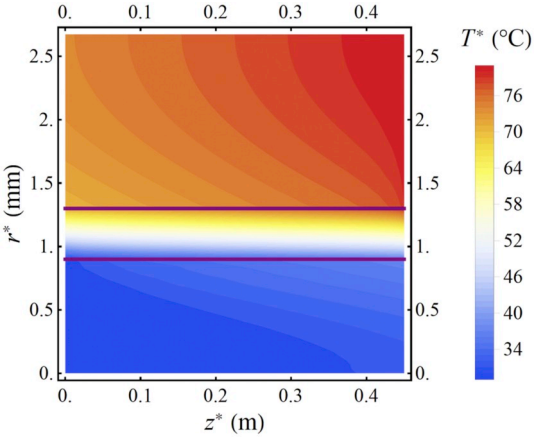

Fig. 3. Temperature contours around the hollow-fiber wall for UFRJ desalination unit. For inlet temperatures of the water in the lumen and in the shell of 30 °C and 80 °C, respectively. Purple horizontal lines are included to represent the lumen- and shell-membrane interfaces. (For interpretation of the references to colour in this figure legend, the reader is referred to the web version of this article.)

especially for smaller temperatures of the shell side, substantiating the use of the model and solution methodology to predict the behavior of hollow-fiber DCMD modules. Moreover, the procedure developed in the present work offers a good estimate of experimentally determined distilled water flux values [22], in spite of the possible shortcomings of a simplified, single-fiber model.

The left column of Table 1 presents the value of the parameters for the UFRJ desalination unit containing 350 fibers in a vessel with 100 mm and 450 mm in internal diameter and effective length, respectively. The water in the lumen is considered to be completely free of ions, whilst the feedwater contains 2.5 wt% of NaCl. Fig. 2b depicts the predicted effect of the feed temperature on the distilled water flux for this system for an inlet permeate temperature of 30 °C. An exponential-like curve is obtained, as expected from the expression for the partial pressure of water vapor from Eq. (8.e). A comparison of these results with the ones from Fig. 2a shows that the performance of the UFRJ desalination unit is within the same order of magnitude as other systems reported in the literature. In fact, the distilled water flux for the UFRJ desalination unit could be even higher if the same inlet permeate temperature as from Wang et al. (2008) [22] was used (17 °C), given the direct relation between the water flux and the partial pressures difference. Fig. 3 presents temperature contours for the UFRJ desalination unit for an inlet feed temperature of 80 °C (feed flow entering at the top-right portion of the graph), while the inlet permeate temperature is maintained at 30 °C (permeate flow entering at the bottom-left portion of the graph). Purple horizontal lines delimit the membrane region, where significant temperature gradients are present, in accordance with the insulating properties of the membrane.

Fig. 4a displays the local distilled water flux across the membrane

Table 1
Sensitivity analysis for the hollow-fiber membrane module of the UFRJ desalination unit.

	Nominal	Nominal - 10%		Nominal + 10%	
	Distilled water flux (L/m^{2}h)	Distilled water flux (L/m^{2}h)	Gain	Distilled water flux (L/m^{2}h)	Gain
Internal radius of the membrane = 0.9 mm	17.4	16.0	−8.05%	19.4	+11.5%
Outer radius of the membrane = 1.3 mm	17.4	21.3	+22.4%	14.8	−14.9%
Membrane pore diameter = 0.2 μm	17.4	16.6	−4.60%	18.1	+4.02%
Membrane porosity = 0.8	17.4	11.9	−31.6%	25.0	+43.7%
Thermal conductivity of the membrane polymer = 0.16 W/mK	17.4	17.5	+0.57%	17.3	−0.57%
Flow rate in the fibers = 1.0 m^3/h	17.4	17.4	0%	17.4	0%
Flow rate in the shell = 0.6 m^3/h	17.4	17.1	−1.72%	17.6	+1.15%

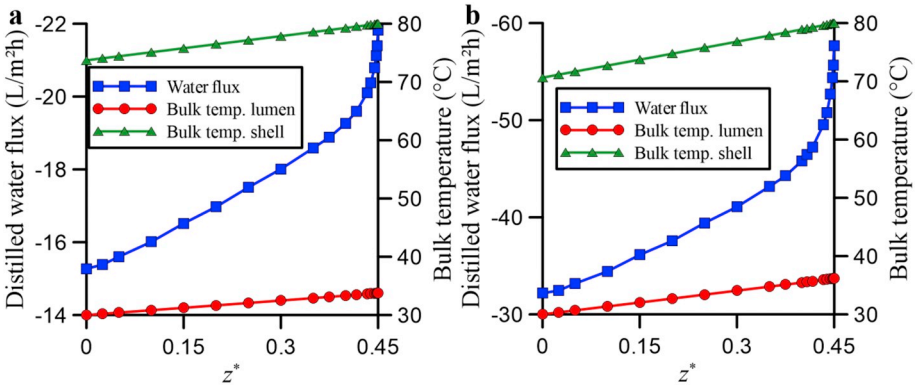

Fig. 4. Behaviors of the distilled water flux on the lumen side and bulk temperatures along the longitudinal position. Results for inlet temperatures of the water in the lumen and in the shell of 30 °C and 80 °C, respectively, for the following modules: (a) UFRJ desalination unit; (b) best combination of the parameters studied.

for the UFRJ desalination unit at the same conditions used to construct Fig. 3. A spike of the magnitude of the water flux is present towards the entrance of the feed flow. This behavior stems from the exponential relation between the partial pressure and the temperature, i.e., the point with the highest feed temperature at the interface with the membrane has the largest distilled water flux. The bulk temperatures for the two flows adjacent to the membrane are also present in Fig. 4a. The behaviors of both curves are approximately linear and, given the insulating properties of the membrane, a great portion of the heat transferred between flows is carried with the water vapor flow across the membrane. The heat gained by the permeate flow and the heat lost by the feed flow are compared, and their magnitude is approximately equal to 4.3 kW, further verifying the adequacy of the model and solution methodology proposed. This heat transfer figure allows the prediction of energy expenditure to distill water for the UFRJ desalination unit, at the simulated conditions, of 275 kWh/m^3.

In face of this poor predicted performance of the UFRJ desalination unit from an energy efficiency standpoint, a sensitivity analysis of the distilled water flux with the main parameters of the system is carried out. The results are shown in Table 1. The nominal values for the parameters are presented in the left column and 10% is either added or subtracted from the nominal value to perform the sensitivity analysis. From the results, it is possible to assert that the membrane morphology and size play a major role in the performance of the hollow-fiber DCMD module under analysis, with a porosity increase rendering a ~44% higher permeate water flux across the membrane. These findings stress the importance of developing porous membranes tailor designed for DCMD applications, which shall be pursued in future works. On the other hand, the flow rate and the thermal conductivity of the polymer have only a marginal effect on the predicted distilled water flux.

In order to test the performance achievable through the enhancement of the desalination system, a hypothetical desalination unit was simulated, with either 10% added or subtracted (whichever enhances the water flux) from each of the nominal parameters of the UFRJ desalination unit. For this case, the mean magnitude of the distilled water flux becomes 39.2 L/m^2 h, a 125% enhancement in comparison with the originally assembled UFRJ desalination unit for a feed temperature of 80 °C. Fig. 4.b illustrates the variation of the distilled water flux across the membrane and the bulk temperatures at both sides of the membrane with the longitudinal position along the module for this hypothetical DCMD unit. Once again the water flux soars near the entrance of the feed flow for the same reasons previously described. The magnitudes of the water fluxes are much higher as well. From the bulk temperatures, the magnitude of the heat transferred between the two flows is evaluated as approximately 7.1 kW, thus decreasing the energy expenditure predicted to roughly 200 kWh/m^2.

4. Conclusions

The hybrid numerical-analytical approach combining the GITT with a single domain reformulation was successfully employed in the solution of a simple single-fiber model of a hollow fiber-based membrane module for water desalination. The developed procedure generated results for the distilled water flux that agreed well with both experimental and numerical results previously published for this configuration. In addition, a set of predictions for the available desalination unit at UFRJ was also offered, and a fairly large value for the energy expenditure to desalinate water was found (275 kWh/m^3). A sensitivity analysis was done to indicate a path for possible improvement in the design of the DCMD module, showing that marked enhancement of the distilled water flux can be achieve through careful selection or design of membranes for DCMD. In addition, a configuration with predicted energy expenditure of 200 kWh/m^3 was simulated, demonstrating that the improvements also positively affect the energy efficiency of the module.

Acknowledgements

The authors would like to acknowledge the partial financial support provided by CNPq (projects no. 380282/2019-4 and 142098/2015-9), FAPERJ, and CAPES, all of them sponsoring agencies in Brazil.

References

[1] Y. Ammar, S. Joyce, R. Norman, Y. Wang, A.P. Roskilly, Low grade thermal energy sources and uses from the process industry in the UK, Appl. Energy 89 (2012) 3–20, https://doi.org/10.1016/j.apenergy.2011.06.003.
[2] N. Voutchkov, Energy use for membrane seawater desalination – current status and trends, Desalination 431 (2018) 2–14, https://doi.org/10.1016/j.desal.2017.10.033.
[3] A. Alkhudhiri, N. Darwish, N. Hilal, Membrane distillation: a comprehensive review, Desalination 287 (2012) 2–18, https://doi.org/10.1016/j.desal.2011.08.027.
[4] A.K. Fard, Membrane Distillation Desalination: An Emerging Technology, 1st ed., Lambert Academic Publishing, 2013.
[5] B.B. Ashoor, S. Mansour, A. Giwa, V. Dufour, S.W. Hasan, Principles and applications of direct contact membrane distillation (DCMD): a comprehensive review, Desalination 398 (2016) 222–246, https://doi.org/10.1016/j.desal.2016.07.043.
[6] N. Dow, S. Gray, J.-D. Li, J. Zhang, E. Ostarcevic, A. Liubinas, P. Atherton, G. Roeszler, A. Gibbs, M. Duke, Pilot trial of membrane distillation driven by low grade waste heat: membrane fouling and energy assessment, Desalination 391 (2016) 30–42, https://doi.org/10.1016/j.desal.2016.01.023.
[7] A. Cipolina, M. Di Sparti, A. Tamburini, G. Micale, Development of membrane distillation module for solar energy seawater desalination, Chem. Eng. Res. Des. 90 (2012) 2101–2121, https://doi.org/10.1016/j.cherd.2012.05.021.
[8] M. Khayet, J.I. Mengual, T. Matsuura, Porous hydrophobic/hydrophilic composite membranes: application in desalination using direct contact membrane distillation, J. Membr. Sci. 252 (2005) 101–113, https://doi.org/10.1016/j.memsci. 2004.11.022.
[9] S. Srisurichan, R. Jiraratananon, A.G. Fane, Mass transfer mechanisms and transport resistances in direct contact membrane distillation process, J. Membr. Sci. 277 (2006) 186–194, https://doi.org/10.1016/j.memsci.2005.10.028.

[10] Ó. Andrjesdóttir, C.L. Ong, M. Nabavi, S. Paredes, A.S.G. Khalil, B. Michel, D. Poulikakos, An experimentally optimized model for heat and mass transfer in direct contact membrane distillation, Int. J. Heat Mass Transf. 66 (2013) 855–867, https://doi.org/10.1016/j.ijheatmasstransfer.2013.07.051.
[11] A.S. Kim, Cylindrical cell model for direct contact membrane distillation (DCMD) of densely packed hollow fibers, J. Membr. Sci. 455 (2014) 168–186, https://doi.org/10.1016/j.memsci.2013.12.067.
[12] R.M. Cotta, Integral Transforms in Computational Heat and Fluid Flow, 1st ed., CRC Press, Boca Raton, FL, 1993.
[13] R.M. Cotta, D.C. Knupp, C.P. Naveira-Cotta, Analytical Heat and Fluid Flow in Microchannels and Microsystems, Mechanical Eng. Series, Springer-Verlag, New York, NY, 2016.
[14] D.C. Knupp, R.M. Cotta, C.P. Naveira-Cotta, S. Kakaç, Transient conjugated heat transfer in microchannels: integral transforms with single domain formulation, Int. J. Therm. Sci. 88 (2015) 248–257, https://doi.org/10.1016/j.ijthermalsci.2014.04.017.
[15] A.P. Almeida, C.P. Naveira-Cotta, R.M. Cotta, Integral transforms for transient three-dimensional heat conduction in heterogeneous media with multiple geometries and materials, Paper # IHTC16-24583, Proc. of the 16th International Heat Transfer Conference – IHTC16, Beijing, China, August 10th–15th, 2018.
[16] K.M. Lisboa, R.M. Cotta, Hybrid integral transforms for flow development in ducts partially filled with porous media, Proc. R. Soc. A 474 (2018) 20170637, https://doi.org/10.1098/rspa.2017.0637.
[17] K.M. Lisboa, R.M. Cotta, On the mass transport in membraneless flow batteries with flow-by configuration, Int. J. Heat Mass Transf. 122 (2018) 954–966, https://doi.org/10.1016/j.ijheatmasstransfer.2018.02.002.
[18] K.M. Lisboa, J. Su, R.M. Cotta, Single domain integral transform analysis of natural convection in cavities partially filled with heat generating porous medium, Numer. Heat Tran. Appl. 74 (2018) 1068–1086, https://doi.org/10.1080/10407782.2018.1511141.
[19] T.M.N. Lopes, Caracterização experimental de um dessalinizador de água por membrana polimérica, Final Graduation Project (In Portuguese), Mechanical Engineering Dept, Polytechnic School, POLI/UFRJ, Rio de Janeiro, Brazil, 2018.
[20] J. Phattaranawik, R. Jiraratananon, A.G. Fane, Heat transport and membrane distillation coefficients in direct contact membrane distillation, J. Membr. Sci. 212 (2003) 177–193, https://doi.org/10.1016/S0376-7388(02)00498-2.
[21] IMSL Library, Rogue Wave Software, Visual Numerics, Boulder, 2010.
[22] K.Y. Wang, T.-S. Chung, M. Gryta, Hydrophobic PVDF hollow fiber membranes with narrow pore size distribution and ultra-thin skin for the fresh water production through membrane distillation, Chem. Eng. Sci. 63 (2008) 2587–2594, https://doi.org/10.1016/j.ces.2008.02.020.